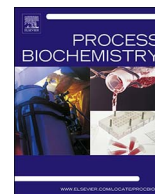




Contents lists available at ScienceDirect

Process Biochemistry

journal homepage: [www.elsevier.com/locate/procbio](http://www.elsevier.com/locate/procbio)

# Monitoring complex monosaccharide mixtures derived from macroalgae biomass by combined optical and microelectromechanical techniques

Alexandra Chudnovsky<sup>a,\*</sup>, Alexander Golberg<sup>b</sup>, Yoav Linzon<sup>c</sup>

<sup>a</sup> Raymond and Beverly Sackler Faculty of Exact Sciences, School of Geosciences, Tel-Aviv University, Tel-Aviv 69978 Israel

<sup>b</sup> Porter School of Environmental Studies, Tel Aviv University, Tel Aviv 69978, Israel

<sup>c</sup> School of Mechanical Engineering, Tel Aviv University, Tel Aviv 69978, Israel

## ARTICLE INFO

### Keywords:

Biorefinery  
Reflectance spectroscopy  
Micro- and nano-electromechanical systems (MEMS/NEMS)  
Monosaccharide mixtures

## ABSTRACT

To foster the development of macroalgal biomass for biorefinery applications, we tested two orthogonal techniques for rapid phenotyping of the green macroalga *Ulva* based on its glucose, rhamnose, xylose and glucuronic acid contents as derived for reference by acid hydrolysis. Partial Least Squares (PLS) regression analyses, calculation of slopes and correlations across different spectral ranges/frequencies were used to predict the monosaccharide contents using two complementary methods: near infrared reflection spectroscopy (NIRS) and microelectromechanical systems (MEMS) resonating membrane vibrometry. Both methods were found to perform sufficiently well in monosaccharide mixtures and to enable quantitative assessment of different monosaccharide contents with the relative Root Mean Square Error of Prediction (%RMSEP) ranging from 8 to 16% (with similar accuracy when using PLS analyses). The best estimation was found for rhamnose and glucose contents, whereas xylose and uronic acid content predictions were found to be less accurate using PLS analyses. For the two latter components, slopes across different spectral ranges and frequencies at certain signals provided better estimates for their concentrations (e.g. for NIRS slopes:  $R^2$  values in the range 0.55–0.66 and with higher accuracy for MEMS: between 0.75 and 0.90). This result is pivotal for opening new perspective to the construction of simple, multi-functional sensors for biomass downstream processing control in biorefinery and biometric applications.

## 1. Introduction

Bioeconomy provides a possible solution for the demand on the natural resources by substitution of the nonrenewable resources with resources derived from biomass [1]. A fundamental unit that will enable the bioeconomy implementation is biorefinery. Biorefinery is a collective term for the complex system that includes biomass production, transportation, conversion into products and distribution. A key component of biomass is its monosaccharide content. Monosaccharides can be directly used in food, cosmetic and industrial applications, such as batteries and paper, or, alternatively, they can be fermented by microorganisms to advanced products including biofuels. Biomass composition is very diverse and each of the composing monosaccharides has its own industrial applications and market values. In addition, the structure and relative abundance of the monosaccharides predicate the downstream processing for fractionation, purification and fermentation [2]. Because of the vast diversity in the chemical composition of the macroalgae biomass feedstock for biorefinery [3], there is a clear need for methods for rapid quantification of monosaccharides in the biomass

or its derived intermediate products. Upon widespread availability, these methods will enable rapid process adaptation for the variation in the raw material input, thus increasing energetic and environmental efficiency.

Reflectance spectroscopy of solid particles in the VIS-NIR-SWIR region (400–2400 nm) is a well known technique by which a material chemical composition can be rapidly and quantitatively assessed [4–6]. Since the late 1970s, qualitative and quantitative applications of near infrared spectroscopy (NIRS) in various fields including pharmaceutical [7], food [8], textile industries [9], and fresh plants [10] have grown dramatically. In macroalgae, spectral signatures based on absorption features are indicative of the macroalgal type and condition [11]. The synergy of multivariate statistical methods (such as Partial Least Squares Regression (PLS) and Principle Component Analyses (PCA)) is very useful for extracting quantitative information from NIR spectroscopy. For example, dry matter, nutrient content, oil, protein, salinity and plant diseases have been accurately estimated in fresh vegetation samples. NIR spectral range (700–2500 nm) in combination with regression analyses was implemented to study sugar concentrations in

\* Corresponding author.

E-mail address: [achudnov@post.tau.ac.il](mailto:achudnov@post.tau.ac.il) (A. Chudnovsky).

<https://doi.org/10.1016/j.procbio.2018.01.018>

Received 18 November 2017; Received in revised form 11 January 2018; Accepted 24 January 2018  
1359-5113/ © 2018 Elsevier Ltd. All rights reserved.

fruits (e.g. apples, mango, passion fruit), vegetables (e.g. potato, sugar beet) and dry cakes [12–16]. Interestingly, Oliveira et al. [14] found that NIR spectroscopy was superior in determination of total acid content, while the best results for glucose, fructose, sucrose, total sugar and citric acid contents were obtained using mid-infrared spectral range. Rady and Guyer [15] highlighted on a potential of using selected wavelengths to estimate sugar content in potatoes. In the last decade, many studies also focus on the applicability of using NIRS for biomass analyses and biomass processing monitoring [17–19]. For example, [19] built multispecies feedstock models for composition, as well as monosaccharide release and yield.

Extensive research has been also conducted in using light spectroscopy in the field of macroalgae biomass characterization (e.g. [10,20–22]). Robic et al. [23] applied PLS regression using reflectance measurements to characterize the chemical composition of Ulvan, a major polymer of *Ulva*, common cosmopolitan green macroalgae, with functional properties, making it viable for Ulvan industrial production. Shefer [24] explored the direct *Ulva* biomass monosaccharides phenotyping based on spectral slopes and spectral index analyses of monosaccharides, where low and high contents of glucose, rhamnose, xylose and glucuronic acid from fresh and dried tissues of *Ulva fascinata* were successfully distinguished.

Micro- and nano-electromechanical systems (MEMS/NEMS) devices operating near vibrational resonance are emerging tools in chemical analysis [25–27], where high sensitivity and selectivity to specific components is potentially unlimited [26,28–30]: for example, recently in-line piezoelectric MEMS cantilever resonators have been used to monitor the sugar composition in wine fermentation process [31]. Surface defined chemical characterization can thus provide for a powerful tool augmenting far-field optical characterization techniques. While very large scale integration (VLSI) of MEMS/NEMS resonator arrays for fast chemical analysis has been proven as viable [32], some caveats still exist. The most central practical problem with the deployment of MEMS/NEMS devices, specifically occurring in dynamic rather than static wet ambient operation [33], is the strong dependence of the measurement on the cleanliness of the sensor surface, limiting both actuation efficiency and quality factors below their theoretical limits [34,35]. This has been overcome with the use of open-gap (single-film co-located electrode) [36] rather than close-gap [37] membrane resonator geometry. In the latter geometry for micro-membranes, operation in harsh aqueous conditions is achieved in single-layer membrane geometry [38]. In the current paper, rather than using multiplexed physical arrays of MEMS resonators with different characteristics (e.g., geometry or coating), a singular membrane is used in exposure to the sugar complexes, and the measured spectra are analyzed with advanced statistical methods in conjunction with the NIRS characterizations.

Macroalgae are an emerging sustainable feedstock for biorefineries [39]. However, macroalgae feedstock show a large variation and diversity of the composing monosaccharides, making it a challenging feedstock for biorefinery. In the previous work we showed that adaptation of the microorganism number and type to specific monosaccharides composition of the fermenting media increases the efficacy of monosaccharides conversion to bio-ethanol [2]. However, rapid determination and quantification of monosaccharides in the macroalgae biomass hydrolysates, prepared for fermentation are lacking. In this work, we exemplify the application of two complementary methods on the monosaccharides determination in the green macroalgae *Ulva* hydrolysates, a potential input material for multiple fermentation processes [27]. Our goal is therefore to rapidly quantify the monosaccharide content in the acid hydrolysates of the *Ulva* biomass. Rapid quantification of the major monosaccharides in the hydrolysates will allow adaptation of fermentation processes to increase the conversion efficiency.

## 2. Materials and methods

We used two complementary methods to predict the monosaccharide contents: near infrared reflection spectroscopy (NIRS) and microelectromechanical (MEMS) resonating membrane vibrometry.

### 2.1. Monosaccharide and sugar acid content determination with ion chromatography

Macroalgae from *Ulva* genus were collected in Tel Aviv, Israel in May 2015. The biomass dried in an oven at 40 °C until constant weight. The dried biomass was made brittle by liquid nitrogen and then grinded into powder manually in a mortar. The *Ulva* powder was sieved by 30 mesh sieve to make sure all particle sizes are smaller than 0.5 mm. All chemicals and standards were purchased from Sigma–Aldrich (Israel) if not otherwise mentioned.

Thermochemical deconstruction for monosaccharides release was conducted in 10 mL centrifuge tubes (Nalgene™ Oak Ridge High-Speed PPCO, Thermo-Fisher Scientific, CA) in autoclave (Tuttnauer 2540MLV, Netherlands). For each batch, dried samples of *Ulva* were weighed on analytical balance (Mettler Toledo, Switzerland), sulfuric acid (Sigma–Aldrich, Israel) was injected into the tube and the mix was vortexed to make the powder well distributed in acid. After deconstruction, the hydrolysates were neutralized by sodium hydroxide (Sigma–Aldrich, Israel). All the solid/liquid ratio, acid concentrations, hydrolysis time and temperature are shown in Table 1.

Dionex ICS-5000 platform (Thermo Fischer Scientific, MA, USA) was used to quantify released monosaccharides in hydrolysate. We used standard HPLC method for sugar analysis in the biomass hydrolysate [40]. CarboPac MA1 and its corresponding guard column were used for separation. An electrochemical detector with AgCl was used as reference electrode for detection. A ternary solvent system was used for elution as shown in Table 2. The column temperature was kept at 30 °C and the flow rate was set to 0.4 mL min<sup>-1</sup>. Calibration curves were produced for rhamnose, glucose, xylose and glucuronic acid on gradient to determine the concentration of corresponding substances in the hydrolysate. All uronic acid peaks were integrated and calculated accordingly using the calibration curve of glucuronic acid (UA) for estimation. The concentrations of the rest of the released monosaccharides were negligible. For spectral analysis 10 μL of hydrolysates was dried at 40 °C on the microscope glass.

### 2.2. Optical and mechanical measurements

For NIRS analyses, we conducted a preliminary study to determine the best background on which to trap the monosaccharide released

**Table 1**  
Protocols used for *Ulva* biomass deconstruction to monosaccharides.

#j	T (°C)	Time (min)	%Acid	%Solid
1	100	30	0	5
2	100	45	0.5	15
3	100	60	2	25
4	100	45	5	5
5	121	30	0.5	25
6	121	45	0	15
7	121	60	5	5
8	121	30	2	15
9	134	30	2	25
10	134	45	5	25
11	134	60	0	15
12	134	60	0.5	5
13	134	30	5	15
14	121	45	2	5
15	100	60	0.5	15
16	134	45	0	25

**Table 2**  
Ion chromatography protocol for *Ulva* hydrolysates.

Time (min)	A (water)	B (480 mM NaOH)	C (1 M NaAcO)
0	94%	6%	0%
10	52	8	40
12	22	8	70
18	20	80	0
20	94	6	0

from the microalgae with acid hydrolysis. In previous studies, it was found that the optimal configuration for spectral analysis is a glass disk (2 mm thick) with a black carbon background, placed underneath [41–43] (Fig. 1(a)). Measuring the reflectance of the dry samples placed above the glass maximizes any meaningful material spectral response. Traps with dried monosaccharide were measured by attaching the high intensity contact probe device (“potato”) to the sample and extracting an average of 40 readings, using bare fiber and self-probed illumination. The “potato” was set on a stable tripod base and maintained in a constant position at a nadir-observing angle. For all experiments halon in the same geometry was used as a white reference to enable conversion of the measurement data to reflectance values. Samples were scanned by an Analytical Spectral Devices (ASD) Full-Range (FR) spectrometer (Analytical Spectral Devices, Boulder, CO, USA). The FR spectrometer samples a spectral range of 350–2500 nm. The instrument uses three detectors spanning the visible and near infrared (VNIR, comprised of Si photodiode array) and shortwave infrared (SWIR1 and SWIR2, comprised of two separate InGaAs photodiodes).

For MEMS characterization, spectra were acquired before, during, and after application of liquid droplets of biomass hydrolysate on top of the membrane surface injected with a micro-pipette, for subsequent analysis. Using background before each wet measurement, wet condition measurement, and subsequent cleaning of the membrane measurement trap (drying with a vacuum pump), the loaded mass and stiffness changes alter the resonant frequency value within the band. In

frequency-domain characterization, the Si membrane resonators (100  $\mu\text{m}$  diameter, see Fig. 1(c) and (d)) are operated in flexure at the fundamental vibration mode. A photodetector collects the reflected light (Fig. 1(c)) into the network analyzer feedthrough, sweeping the frequency band in synchrony with the excitation. A Laser Doppler Vibrometer (LDV) setup is used in velocity mode, where the measured voltage is calibrated to velocity in mm/s [26,27]. The sample was loaded with 1  $\mu\text{L}$  of liquid droplet centered on the membrane from above.

Note that for NIRS analyses we used dried hydrolysates. Since the light diffusion is much greater across 1100–2400 nm, spectra are more sensitive to factors that influence light diffusion such as physical structure and the presence of water in the sample [44]. The change in absorption depth around 1400 and 1900 nm is particularly deep for wet samples. Water has a broad absorption range centred around 1400 and 1940 nm that masks other absorption features associated with constituents such as nitrogen, monosaccharides and cellulose.

### 2.3. Statistical analysis: Partial Least Squares (PLS) regression

The multivariate calibration models were generated using Partial Least Squares (PLS) regression, with the goal of defining a relationship between the reflectance/frequency signals of samples and their monosaccharide concentration (in units of  $\mu\text{g mL}^{-1}$ ):

$$Y = A + A_1X_1 + A_2X_2 + A_3X_3 + \dots + A_nX_n \quad (1)$$

where  $Y$  is the monosaccharide concentration of a sample,  $A$  is an empirical coefficient, and  $X$  is the reflectance/frequency at a specific wavelength.

For NIRS, to simplify the spectral signals in order to ensure stable calibration and to improve the predictive ability of the final model, we applied different pretreatments in the spectral domain. Calibration models were computed using the entire range of VIS-NIR-SWIR, selected wavelengths as well as using raw (reflectance), first- and second derivative transformed data. Additionally, in order to minimize the

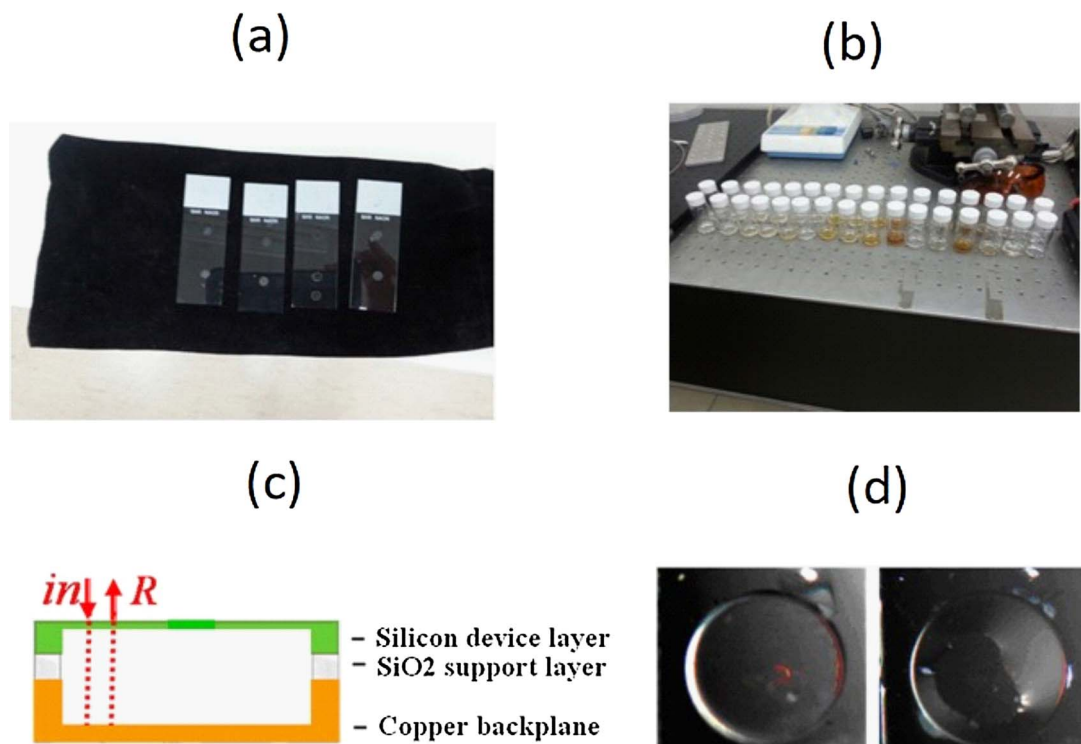


**Fig. 1.** (a) Monosaccharide release placed above black carbon background and dried for 24 h. (b) Glasses and pipette of glucose solutions used in vibrating MEMS characterizations. (c) Schematic of membrane cross-section, with layer composition and arrows indicating probing light (related to LDV apparatus characterizing vibrations). (d) Images of membrane surface used for vibrating MEMS measurement (100  $\mu\text{m}$  diameter), taken before (left, reference) and after (right) application of sugar solution on the membrane surface.

effect of the glass background, we calculated Spectral Ratio ( $RI$ ) by calculating the apparent ratio values for each waveband, taking the single-beam spectrum against that of the glass background, as follows:

$$RI(\lambda) = \frac{B_{rad}(\lambda)}{B_{background}(\lambda)} \quad (2)$$

where  $B_{rad}(\lambda)$  is the reflectance of the dried monosaccharide, plus the reflectance of the glass trap itself, and the reflectance of the black carbon background on which the glass trap sits, and  $B_{background}(\lambda)$  is reflectance of the clean glass and that of the top of the black carbon background. The same pre-treatments that were applied on the raw original spectra were tested also on the  $RI$  transformations. In order to limit the set of combinations to a manageable number, we kept both the number and identity of glass traps constant in both calibration and validation stages, changing only the pre-processed procedure.

For MEMS, the frequency response signals were normalized, and the difference between the spectra measured in wet conditions and the background spectra were calculated from the spectra measured in the presence of deposited liquid monosaccharide mixture. Similarly to NIRS, we used different pre-processing techniques (first and second derivatives), as well as estimating the correlation between resonant frequency and different monosaccharide contents. Multivariate calibration models were calculated by PLS regression.

The predictive capability of all models using both techniques was compared in terms of the relative standard error for both calibration and validation sets (denoted as RMSEC (%) and RMSEP (%), respectively).

RMSEP is defined as square root of the average of the squared differences between predicted and measured values of the validation objects [45]:

$$RMSEP = \sqrt[2]{\frac{\sum (X_m - X_p)^2}{n_v}} \quad (3)$$

where  $X_m$  is the measured sample concentration,  $X_p$  is the predicted value of the sample on the basis of spectral analysis,  $n_v$  is the number of samples in the calibration stage, and the summation is performed over the whole sample range  $1 < i < n_v$ . The predictive capability of all models was compared in terms of the relative standard error for both the calibration and validation sets (denoted as RMSECV (%) and RMSEP (%)), where the former is defined as:

$$RMSECV(\%) = \sqrt[2]{\frac{\sum (X_m - X_p)^2}{\sum X_m^2}} \times 100 \quad (4)$$

The accuracy of each calibration model was evaluated based on the coefficient of determination ( $R^2$ ) for predicted versus measured values.

Since we have a restricted data set ( $N = 16$ ), we used the most popular “full-cross-validation” method, where only one sample at a time is kept out of the calibration and used for prediction (also termed as the “leave one sample out procedure”). Lowest RMSEP (%) and highest  $R^2$  values were selected as criteria to indicate optimal model performance and the values generated from the validation set were used to choose the best data pre-processing technique. Additionally, best models were chosen based on decreasing of residual variance observed on the  $X$ -axis. PLS analyses and different spectral pretreatments were performed using Unscrambler software, Version 9.1 (Camo, Norway, 2004) and SAS software.

#### 2.4. Statistical analysis: the impact of individual wavelengths and slopes across different spectral ranges

In this study we also investigated the influence of using the whole spectral region as well as selecting individual wavelengths to generate an optimal PLS model to predict monosaccharide concentrations. Martens’ uncertainty test is a significance testing method that can be implemented when using cross validation PLS method, which assesses the stability of Regression results and the selection of significant  $X$ -variables (Unscrambler, Version 9.1, Camo, Norway, 2004; [45]). Therefore, we first ran our models on the whole wavelength region, and thereafter we applied Martens’ uncertainty test, algorithm in Unscrambler software with the aim of identifying wavelengths that will provide the highest accuracy estimation. Therefore, each model (raw and pre-processed) was first run on the whole range of spectra, and then only significant wavelengths were kept and each model was re-assessed. In addition, the differences in spectral behavior as a function of wavelength, which are indicative of changes in chemical properties, were identified. Importantly, the main criterion for spectral slope selection across the entire spectral range was similar for all samples with different monosaccharide contents. Then, different slopes between a pair of wavelengths were calculated and the most correlative ones were then used in our analyses. The main criteria for slopes and wavelengths selection were the ability to discriminate quantitatively between low vs high monosaccharide content groups as well as selection of spectral ranges that are not impacted directly by strong water absorbance (for NIRS).

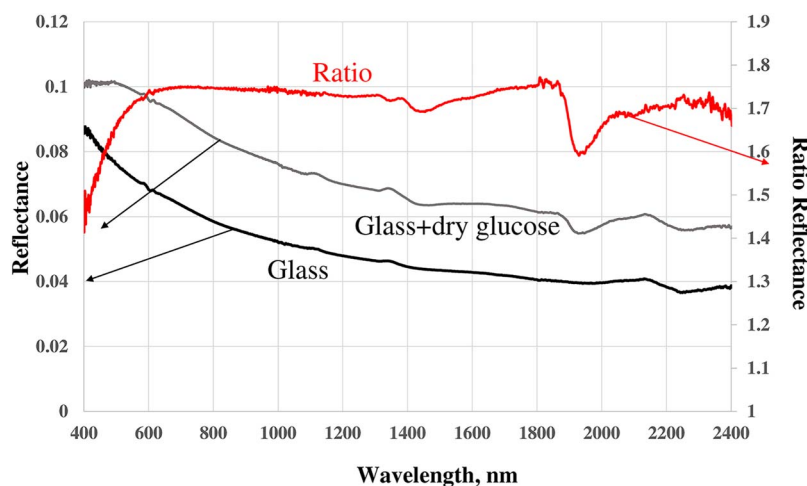


Fig. 2. Reflectance of the glass trap placed on the black carbon background, and reflectance of the dried monosaccharide plus reflectance of glass and black carbon, measured by ASD spectrometer.

**Table 3**  
Major carbohydrates released from dried *Ulva* biomass after thermochemical hydrolysis.

#j	T (°C)	Time (min)	Acid (%)	Solid (%)	Rha ( $\mu\text{g mL}^{-1}$ )	Glc ( $\mu\text{g mL}^{-1}$ )	Xyl ( $\mu\text{g mL}^{-1}$ )	UA ( $\mu\text{g mL}^{-1}$ )
1	100	30	0	5	218.7 $\pm$ 5.2	0.2 $\pm$ 0.1	0.4 $\pm$ 0.1	238.6 $\pm$ 163.6
2	100	45	0.5	15	228.7 $\pm$ 10.3	3.2 $\pm$ 0.1	5.5 $\pm$ 0.125.0	1649.9 $\pm$ 38.4
3	100	60	2	25	3036.1 $\pm$ 51.3	6538.8 $\pm$ 301.5	1339.9 $\pm$ 13.6	16010.4 $\pm$ 1111.5
4	100	45	5	5	1179.1 $\pm$ 13.3	1422.4 $\pm$ 35.5	149.7 $\pm$ 1.9	1058.9 $\pm$ 149.1
5	121	30	0.5	25	49.2 $\pm$ 6.7	4.3 $\pm$ 1.6	4.8 $\pm$ 0.0	942.4 $\pm$ 218.6
6	121	45	0	15	3.0 $\pm$ 0.1	0.001 $\pm$ 0.0	0.0 $\pm$ 0.0	329.7 $\pm$ 277.1
7	121	60	5	5	1215.8 $\pm$ 93.7	1389.3 $\pm$ 89.2	82.9 $\pm$ 29.0	889.5 $\pm$ 22.8
8	121	30	2	15	3739.7 $\pm$ 185.2	5196.2 $\pm$ 124.2	675.6 $\pm$ 29.0	2866.8 $\pm$ 71.6
9	134	30	2	25	6879.6 $\pm$ 43.2	8137.7 $\pm$ 36.6	1054.2 $\pm$ 4.8	3887.0 $\pm$ 21.9
10	134	45	5	25	5218.8 $\pm$ 284.5	7606.6 $\pm$ 253.7	300.4 $\pm$ 3.2	2829.6 $\pm$ 77.7
11	134	60	0	15	3.2 $\pm$ 0.4	0.01 $\pm$ 0.001	0.01 $\pm$ 0.001	211.7 $\pm$ 101.7
12	134	60	0.5	5	976.1 $\pm$ 87	1172.3 $\pm$ 138.3	128.6 $\pm$ 11.7	744.4 $\pm$ 32.4
13	134	30	5	15	3510.8 $\pm$ 445.1	4691.1 $\pm$ 554.9	209.4 $\pm$ 33.7	2120.7 $\pm$ 222.1
14	121	45	2	5	1109.7 $\pm$ 12.3	1255.2 $\pm$ 22.0	142.2 $\pm$ 17.3	836.3 $\pm$ 178.0
15	100	60	0.5	15	10.8 $\pm$ 0.7	0.6 $\pm$ 0.1	0.4 $\pm$ 0.6	456.0 $\pm$ 91.9
16	134	45	0	25	2.9 $\pm$ 0.1	0.01 $\pm$ 0.001	0.01 $\pm$ 0.001	126.0 $\pm$ 17.8

### 3. Results

#### 3.1. Changes in the spectral features as a function of glucose composition

Fig. 2 shows the reflectance of the clean glass and that of the top of the black carbon background (line denoted as “glass”) and reflectance of the dried monosaccharide (settled following two weeks), plus the reflectance of the glass trap itself, and the ratio or subtracted background (denoted as “ratio”).

As seen in Fig. 2, clean dust traps do not exhibit significant absorbance bands across the spectrum, and can therefore be used as a trap for dried monosaccharide characterization.

Next, we quantified the major released monosaccharides from the dried *Ulva* biomass, based on [27]. The results are shown in Table 3. Further, in Fig. 3 we show the reflectance of the ratio spectra of several representative samples with different monosaccharide contents. As can be seen, spectra are characterized by minimal noise and albedo changes with varying dry monosaccharide intensity. For all samples, the baseline up-drift is visible with increasing glucose intensity. This is because as monosaccharide concentration increases, the effect of the dark background in the glass trap diminishes, the reflectance increases and a slope across 400–600 nm changes.

Fig. 4 shows several samples of membranes with wet samples, with high vs low monosaccharide concentrations. As observed, there are high frequency shifts across almost the entire frequency range (except at high frequencies) among samples with different rhamnose content,

resulting from a combination of mass loading, chemical surface adsorption, and tension changes [38]. At high frequencies, low rhamnose samples exhibit ‘flat’ (close to zero) vibration response, whereas larger concentrations exhibit larger signals. This range can be defined as more stable for rhamnose monitoring.

#### 3.2. Slopes vs monosaccharide concentrations using NIRS and MEMS methods

Differences in five spectral ranges indicating changes in monosaccharide concentrations were visually identified and tested across the VIS–NIR–SWIR region (350–2500 nm): 420–600 nm; 600–1000 nm; 1478–1870 nm; 2197–2262 nm and 2262–2364 nm. The coefficient of determination between slope and different monosaccharide concentrations is reported in Table 4. Generally, the slopes increased/decreased with an increasing/decreasing monosaccharide content and can be used as monosaccharide content indicators.

In Fig. 5 we examined frequency vs monosaccharide concentrations. The correlation coefficient is clearly the largest at high frequencies and for all monosaccharide components it is possible to estimate the concentrations.

#### 3.3. PLS analyses

Table 5 shows the best modeling results using PLS analyses run on NIRS data. As can be seen, the best accuracy estimates were achieved

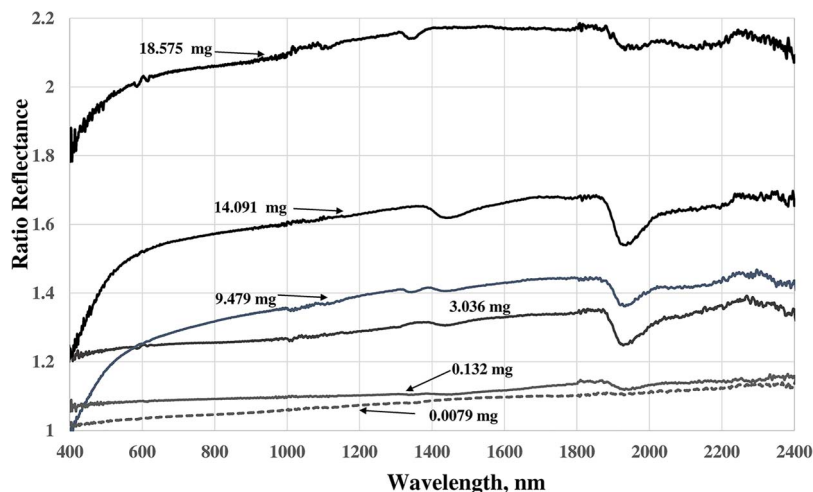


Fig. 3. Baseline up-drift of the spectrum is visible with increasing monosaccharide concentration.

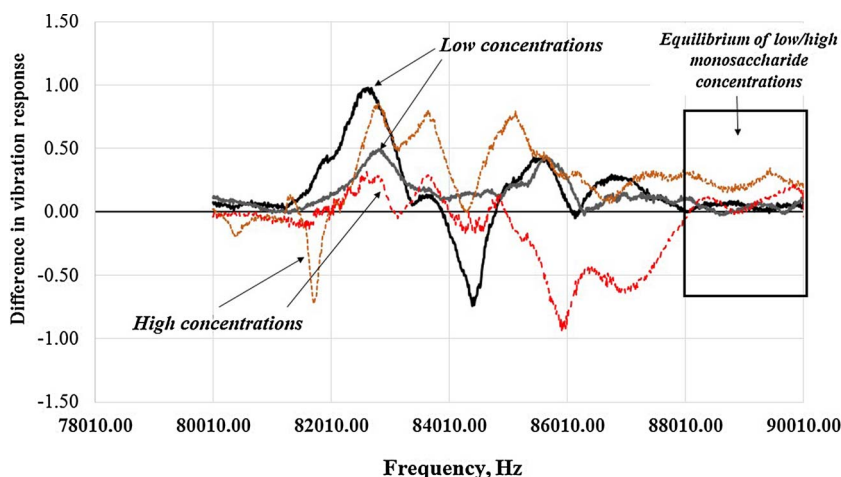


Fig. 4. Electromechanical measurements of monosaccharide content on a vibrating membrane with the subtracted background. Samples 6 and 11 (grey and black) are of low rhamnose contents, whereas samples 9 and 10 (red and brown) are of high rhamnose contents. Box highlights the region of high frequency values where low amounts of monosaccharide concentrations exhibit almost “flat/continuous” signal, which is significantly different from samples with larger concentrations. (For interpretation of the references to color in this figure legend, the reader is referred to the web version of the article.)

Table 4

Coefficient of determination between slopes in selected spectral regions and carbohydrate contents release from the microalgae.

Slope spectral range (nm)	Rha (mg)	Glc (mg)	Xyl (mg)	UA (mg)	Total (mg)	Yield (%)
420–600	0.55	0.59	0.12	0.14	0.48	0.19
2197–2262	0.63	0.63	0.51	0.38	0.64	0.4
2262–2364	0.66	0.61	0.42	0.44	0.67	0.28

when second derivative was applied on the RI spectra run on significant wavelengths, followed by smoothing. Applying this RI model yielded predicted monosaccharide concentrations with a RMSEP of 9.5%, confirming that the model has relatively good predictive ability when operating with five PLS components (Table 5). To give an indication of measured vs predicted values, resulted from our model, we show in Fig. 6, the model results estimated for glucose content as an example. This result indicates that most of the spectral variation observed in our study is indeed related to the monosaccharide concentrations as modeled by the PLS model (and is not being influenced by unknown parameters). Importantly, PLS models were only generated with relatively

high accuracy for glucose and rhamnose contents and much lower  $R^2$  were obtained for glucuronic acid and xylose contents ( $R^2 \approx 0.4$  using second derivative and selected wavelengths as pre-processing technique). Note that a higher percentage of variance explained by a lower number of PLS components indicates model stability.

Different pre-processing techniques were estimated and the best results obtained are summarized in Table 6. Comparing Tables 5 and 6 we can conclude that MEMS performs slightly better than NIRS. However, when using PLS analyses both techniques were unable to estimate uronic acid content with high accuracy.

We note that second derivative applied on frequency, followed by the moving average (to reduce the signal noise), was also found to be accurate to construct the PLS model, but with lower accuracy (these results are not reported in Table 6). As an example of a clear separation between high vs low monosaccharide samples we plot the results of PLS score plot for rhamnose in Fig. 7. As can be seen, the first two LV components explained 74% of the X variance (vibration spectra), and 91% of rhamnose of the Y variance (chemical components). The score plot for the rha model indicated that a significant part of the vibration spectra variations observed in the samples are indeed related to rhamnose, as predicted by the PLS model. Specifically, there is an increasing trend in rhamnose content among samples from left to the

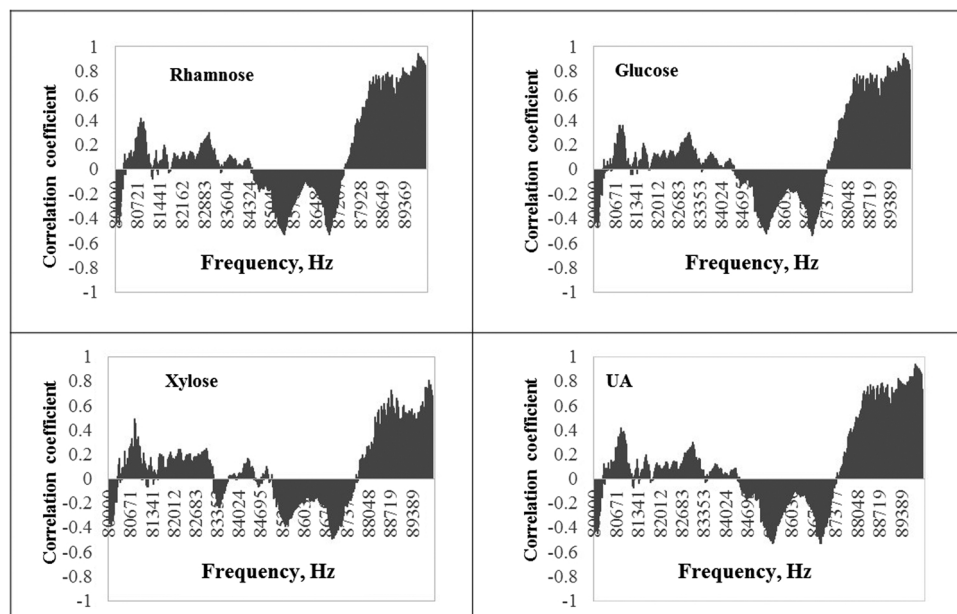


Fig. 5. Correlation coefficient calculated for four monosaccharide components vs frequency at the range 80,000–90,010 Hz (around 80 and 90 KHz).

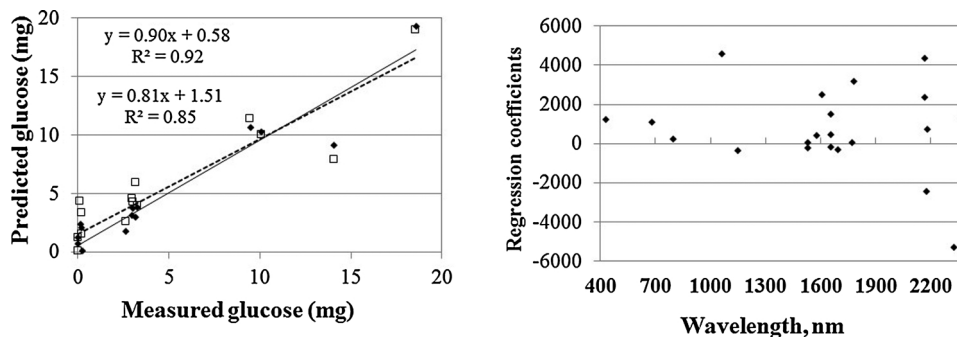


Fig. 6. (a) Measured ( $n = 16$ ) vs. predicted glucose content (% of dry weight) obtained for the best-fit model (second derivative of reflectance spectra when applied on selected wavelengths). (b) Partial Least Squares loadings vectors (LV1-5) for the optimal calibration model as calculated for glucose content from the score plot.

right, indicating that the PLS component models the changes in rhamnose concentrations.

Finally, in Fig. 8 we show important frequencies using Martens uncertainty test to estimate rhamnose contents. Compared with Fig. 5, quite similar ranges were found to be important in its accuracy estimation.

Table 5

Statistical parameters obtained for the calibration stage for each of the Partial Least Squares (PLS) regression models to predict carbohydrate concentrations. RMSECV, root-mean-square error of cross-validation; RPD, ratio of prediction to deviation; #LV, number of LV components (regression coefficients) used to construct the PLS model;  $R^2$ -coefficient of determination and slope (in original values) of the model. Models that were considered are: **2deriv + smoothing (with different number of wavelengths)** (reflectance considered as the second derivative, followed by a smoothing function and run on selected wavelengths); **Slopes**.

Type of model	Type of carbohydrate	Model	#LV	RMSECV/RMSEP	$R^2$	Slope	RPD (calculated for RMSECV only)
Ratio	Glucose	2deriv + smoothing	2	2.5	0.86	0.86	2.5
		(model run on 22 wavelengths)		3.5	0.78	0.83	
	Rhamnose	1deriv + smoothing	5	1.7	0.94	0.93	2.7
		(model run on 28 wavelengths)		2.6	0.93	0.90	
	Xylose	No accurate model was found					
UA	No accurate model was found						
Total		2deriv + smoothing	4	4.5	0.90	0.90	1.7
		(model run on 28 wavelengths)		9.4	0.75	0.85	

Type of model	Type of carbohydrate	Slopes used	$p$ value	RMSE	$R^2$
Slope-based	Glucose	420–600 nm	< 0.0001	2.9	0.88
		1478–1870 nm			
		2197–2262 nm			
		2262–2364 nm			
	Rhamnose	420–600 nm	< 0.0001	2.5	0.87
Xylose		420–600 nm	0.0010	0.43	0.79
		1478–1870 nm			
		2197–2262 nm			
		2262–2364 nm			
UA		420–600 nm	0.02	3.04	0.68
		600–1000 nm			
		1478–1870 nm			
		2197–2262 nm			
Total		420–600 nm	< 0.0001	6.1	0.89
		600–1000 nm			
		1478–1870 nm			
		2197–2262 nm			

**Table 6**

Statistical parameters obtained for the calibration stage for each of the Partial Least Squares (PLS) regression models to predict carbohydrate concentrations. RMSECV, root-mean-square error of cross-validation; RPD, ratio of prediction to deviation; #LV, number of LV components (regression coefficients) used to construct the PLS model;  $R^2$  – coefficient of determination and slope (in original values) of the model. The most accurate models used frequency units run on selected signals.

Type of model	Type of carbohydrate	PLS Model	#LV	RMSECV	$R^2$	Slope	RPD
Frequency	Glucose	Frequency run	3	2.0	0.96	0.92	2.9
		On 7 signals		3.1	0.90	0.85	
Frequency	Rhamnose	Frequency run	3	1.6	0.94	0.89	2.6
		On 9 signals		2.5	0.90	0.85	
Frequency	Xylose	Frequency run	3	0.5	0.90	0.87	2.0
		On 5 signals		0.3	0.78	0.80	
Frequency	UA	No accurate model was found					
Total	Frequency run	On 7 signals	4	5.0	0.88	0.88	1.7
		On 9 signals		9.5	0.70	0.85	

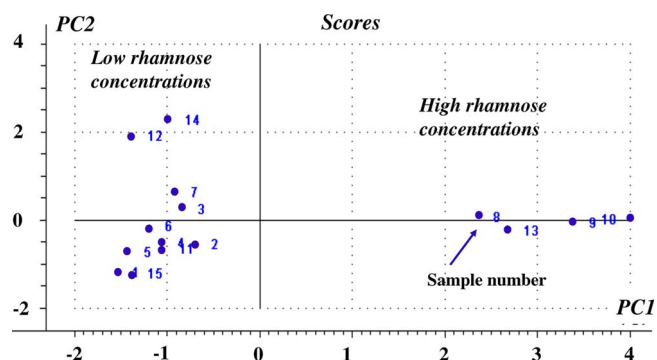


Fig. 7. Score plot for the Partial Least Squares (PLS) model for rhamnose using the most important frequencies (based on Martens test). Arrow indicate the change from left to right in rhamnose content measured in the samples.

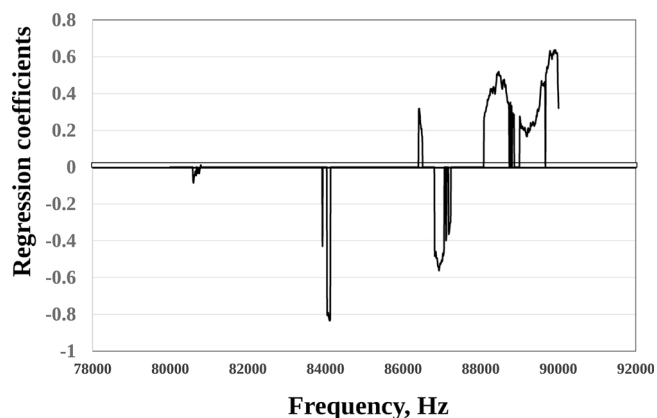


Fig. 8. Important frequencies as identified by PLS regression using Martens uncertainty test to estimate glucose and rhamnose contents using frequency (in Hz).

resonator (MEMS) measurements on a vibrating membrane. Both methods were found to perform sufficiently and to enable quantitative assessment of different monosaccharide contents with the relative Root Mean Square Error of Prediction (%RMSEP) ranging from 6 to 11.5%. The best estimation was found for rhamnose and glucose contents, whereas xylose and uronic acid was found to be less accurate using PLS analyses. For the two latter components, slopes across different spectral ranges and frequencies at certain signals provided better estimates for

their concentrations. This result is encouraging for opening new perspective to construct simple, multi-functional sensors.

Detailed spectroscopic measurements of vegetation were made in the 1960s and 1970s by USDA researchers [46]. These measurements revealed that there are about 42 minor absorption features that can be related to particular foliar chemical concentration. In fact, those features can be categorized as being of either electronic or vibrational origin [47–49]. Absorption bands produced by electronic processes can be clearly distinguished from those produced by vibrational processes. Electronic bands are very broad and shallow that occur mostly in the ultraviolet and extend with diminishing frequency into the visible and near IR (0.4–1  $\mu\text{m}$ ). Vibrational processes produce very sharp and narrow bands that occurs predominantly in the range beyond 2  $\mu\text{m}$ . These processes define the chemical characteristics of the specific compound. For example, absorbencies at 1540 and 1580 nm can be attributed to the presence of starch, cellulose and sugar (due to O–H stretch) [46]. At 1780 nm spectral features are related to the presence of sugar and cellulose (due to C–H and O–H stretching group frequency). Absorbances at 1960 nm and at 2080 nm are attributed to presence of sugar and starch (due to O–H group stretching mode) whereas absorbance at the range 2280 and at 2350 nm related to the presence of starch or cellulose (due to the C–H stretch). In addition, the wavelengths at the range 2100–2300 nm are related to functional groups with aliphatic C–H and phenolic O–H bonds, which could be used to predict the contents of cellulose, lignin, starch and other sugars [46,50]. As can be seen from our results (Fig. 6, right), PLS calibrations on monosaccharide concentrations relied strongly on the 1540 and 1580 nm (O–H stretch), 1780 (C–H/O–H stretching group frequencies), 2160 nm, 2180 nm (C–H, O–H bonds) and 2350 nm (C–H stretch).

As observed in Table 5, using changes in spectral reflectance across different wavelength ranges, all types of monosaccharide concentrations can be estimated with relatively high accuracy. Note, however, that none of our models estimated low concentrations accurately. In this regard, we suggest to expand the data set and include larger number of NIRS method measurements.

As opposed to the NIRS method, in MEMS devices, rather than being sensitive to the chemical molecular monosaccharide structure, the sensitivity is mostly to mass loading (via resonance frequency down-shift), or equivalently to the analyte density, as well as to the average viscosity within the medium (via the resonance broadening) [25,27]. A simplified model for vibrating membranes assuming circular symmetry correlates the central resonance frequency of the  $(m, n)$  mode,  $f_{(m,n)}$ , with the average density  $\rho$  as an inverse-square-root relation via the following equation [27]:

$$f_{(m,n)} = \frac{\alpha_{(m,n)}}{2\pi R} \sqrt{\frac{Y\epsilon}{\rho}} \quad (5)$$

where  $R$  is the membrane radius,  $Y$  is the material Young's modulus ( $\approx 130$  GPa in silicon),  $\epsilon$  is the pre-calibrated tensile stress in the membrane film, and  $\alpha_{(m,n)}$  is a numerical factor associated with the Bessel's function zeros along the membrane modes. Here we chose to work with the mode designated by indices (3, 4). Whereas density characterizations are straightforward via Eq. (5) [27,38], the combined analytical estimation involving density and viscosity, which are both physically characteristic of the immersed liquid [51,52], can be mathematically challenging, as opposed to the statistical approach. In this regard, in our study we used chemometric approach, defined as “The science of relating measurements made on a chemical system or process to the state of the system via application of mathematical or statistical methods” [45]. A main part of chemometrics is multivariate data analysis, which is essential for qualitative and quantitative analysis based on spectral measurements. Combination of both approaches provides important insight into hidden chemical and physical interactions [6,45]. As mentioned in methods, electromechanical spectra of a mixed

signature (e.g. background + liquid sugar) were first normalized using the mean normalization. Then, corresponding background was subtracted from the “mixed” signature signals. These signals for each sample were used as input for our model. The same “background” subtraction was applied to spectral reflectance measurements.

Analyzing Fig. 6(a) and results of all our models, one might conclude that the developed models are less accurate in estimation of low monosaccharide content. To clarify this point, in Table 1S we present average residuals values for several quantitative ranges, from low to high concentrations using PLS models on NIRS and MEMS methods. The ideal case is when the residual value is close to zero (e.g. measured and estimated concentrations are similar). As can be seen, on average, residual values are quite similar between the two examined techniques and for different concentrations. The main reasons for larger residuals can be: (1) the model was run on a relatively small data set; and (2) a small number of samples were used for each quantitative range of monosaccharides. As a result, even extremely small differences between PLS model and the reference values can result in larger residuals and decreased accuracy of the overall model. Generally, the calibration set must span the  $X$  (spectral) space, as well as the  $Y$  (reference) space as widely and representatively as possible [45]. In this regard, in order to derive the practical applications of the presented method, future studies must include a larger number of samples than the one used in this study, with a much wider dynamic range of values (minima and maxima) that is considered important for developing a stable PLS model. In addition, a separate study should be devoted to examine the sensitivity of both techniques to measure the challenging and important low concentrations of monosaccharides.

The results suggest that the two tested methods are potentially useful, both separately and in their multidimensional combination, for estimation of monosaccharide content. Since the method is non-destructive and can measure several constituents quickly, inexpensively, accurately, and simultaneously, it could become a valuable tool for the quality control of low monosaccharide content in *Ulva* and, hence, enable monitoring of the monosaccharide status of plants throughout their growth, both in solution and in powder phases. Liquid versus powder (dried on the glass slide) were powerful for cross validation in correlation with the Dionex 5000 reference readings. In the future all-liquid in-line fluidic quantification of a calibrated device will be easier in the aqueous state rather than the need to dry samples up.

Our results show that when analyses were run on significant wavelengths, better accuracy was achieved. Due to the different chemical interactions and physical properties (such as particle size distribution), the chemical and quantitative information may be obscured by changes in the measured spectra. Therefore, using selected wavelengths was viable for studying monosaccharide concentrations, as also supported by other studies [15,24].

Generally, the selectivity of each monosaccharide should be given with various background of the mixture of monosaccharides. As seen in Table 3 and Fig. 3, each sample contains different quantitative fractions of monosaccharides. Several methods can be used to overcome the disturbances caused by a variety of mixture of monosaccharides. For example, Linear Spectral Unmixing (LSU) is one of the most popular techniques used for analyzing mixed pixels in remote sensing images for numerous applications: geological, agricultural, and land uses quantitative coverage [53–55]. LSU is a procedure by which the measured spectrum of a pixel is decomposed into a collection of spectral “pure” end-members. In our example, pure four end-members are four solutions that contain 100% of each monosaccharide (e.g. rhamnose, glucose, UA and xylose correspondingly). LSU algorithm estimates the relative contribution of each pure end-member (e.g. its fractional abundance) in each sample.

The two approaches presented here for the estimation of the monosaccharide content are perhaps more convenient and user-friendly than traditional approaches (e.g., analytical chemical analyses). Note also that the developed approach is generic and in this study was

demonstrated for macroalgae hydrolysate. A portable spectrometer in combination with an appropriate chemometric model allows many glass traps to be analyzed rapidly in situ by a non-expert operator. Vibrational MEMS elements add to optical characterizations surface capabilities with localized contact information of the sugar composition. This novel instrument can be designed to assess the total quantitative concentration. Moreover, in combination with better sensors, based on multiple channels (including both wavelength and frequencies bands and arrays of devices operating in parallel) or utilizing ground image cameras, this technique can bridge the gap between required methods for rapid and accurate assessment of monosaccharide concentrations in biomass harvesting.

## Acknowledgments

The authors wish to extend gratitude to the anonymous reviewers. Their kind and insightful remarks helped improve our paper greatly.

## Appendix A. Supplementary data

Supplementary data associated with this article can be found, in the online version, at <https://doi.org/10.1016/j.procbio.2018.01.018>.

## References

- [1] J. Enriquez, Genomics and the world's economy, *Science* 281 (1998) 925–926.
- [2] A. Golberg, E. Vitkin, G. Linshiz, S.A. Khan, N.J. Hillson, Z. Yakhini, M.L. Yarmush, Proposed design of distributed macroalgal biorefineries: thermodynamics, bio-conversion technology, and sustainability implications for developing economies, *Biofuels Bioprod. Biorefin.* 8 (2014) 67–82.
- [3] E. Marinho-Soriano, P.C. Fonseca, M.A.A. Carneiro, W.S.C. Moreira, Seasonal variation in the chemical composition of two tropical seaweeds, *Bioresour. Technol.* 97 (2006) 2402–2406.
- [4] W.P. Carey, L.E. Wangen, Determining chemical characteristics of plutonium solutions using visible spectrometry and multivariate chemometric methods, *Chemom. Intell. Lab. Syst.* 141 (1991) 245–257.
- [5] A.R. Coscione, J.C. De Andrade, R.J. Poppi, C. Mello, B. Van Raij, M.F. De Abreu, Multivariate calibration applied to a highly interfering chemical system: the simultaneous spectrophotometric determination of aluminium and iron in plants using xylene orange and partial least-squares regression, *Anal. Chim. Acta* 423 (2000) 31–40.
- [6] M. Otsuka, Comparative particle size determination of phenacetin bulk powder by using Kubelka–Munk theory and principal component regression analysis based on near-infrared spectroscopy, *Powder Technol.* 141 (2004) 244–250.
- [7] E. Dinc, D. Baleanu, F. Onur, Spectrophotometric multicomponent analysis of a mixture of metamizol, acetaminophen and caffeine in pharmaceutical formulations by two chemometric techniques, *J. Pharm. Biomed. Anal.* 26 (2001) 949–957.
- [8] B.G. Osborne, T. Fearn, P.H. Hindle (Eds.), *Practical NIR Spectroscopy with Applications in Food and Beverage Analysis*, Longman Scientific and Technical, 1993.
- [9] M. Blanco, J. Coello, J.M. Garcia Fraga, H. Iturriaga, S. Maspoch, J. Pages, Determination of finishing oils in acrylic fibres by near-infrared reflectance spectrometry, *Analyst* 122 (1997) 777–781.
- [10] A. Moron, D. Cozzolino, Measurement of phosphorus in soils by near infrared reflectance spectroscopy: effect of reference method on calibration, *Commun. Soil Sci. Plant Anal.* 38 (2007) 1965–1974.
- [11] I.E. Ramsey, A. Rangoonwala, M.S. Thomsen, A. Schwarzschild, Flat-plate techniques for measuring reflectance of macro-algae (*Ulva curvata*), *Int. J. Remote Sens.* 33 (2012) 3147–3155.
- [12] A.M.K. Pedro, M.M.C. Ferreira, Simultaneously calibrating solids, sugars and acidity of tomato products using PLS2 and NIR spectroscopy, *Anal. Chim. Acta* 595 (2007) 221–227.
- [13] E. Bobelyn, A.S. Serban, M. Nicu, J. Lammertyn, B.M. Nicolai, W. Saeyns, Postharvest quality of apple predicted by NIR-spectroscopy: study of the effect of biological variability on spectra and model performance, *Postharvest Biol. Technol.* 55 (2010) 133–143.
- [14] G.A. Oliveira, F. Castilhos, C. Renard, S. Bureau, Comparison of NIR and MIR spectroscopic methods for determination of individual sugars, organic acids and carotenoids in passion fruit, *Food Res. Int.* 60 (2014) 154–162.
- [15] A. Rady, D. Guyer, R. Lu, Evaluation of sugar content of potatoes using hyper-spectral imaging, *Food Bioprocess Technol.* 8 (2015) 995–1010.
- [16] L. Pan, Q. Zhu, R. Lu, J.M. McGrath, Determination of sucrose content in sugar beet by portable visible and near-infrared spectroscopy, *Food Chem.* 167 (2015) 264–271.
- [17] F. Xu, D. Wang, Rapid determination of sugar content in corn stover hydrolysates using near infrared spectroscopy, *Bioresour. Technol.* 147 (2013) 293–298.
- [18] A. Pandey, S. Negi, P. Binod, C. Larroche, *Analysis of Lignocellulosic Biomass Using Infrared Methodology*, Chapter 2: Pretreatment of Biomass, Elsevier, Amsterdam,

- 2015.
- [19] C.E. Payne, E.J. Wolfrum, Rapid analysis of composition and reactivity in cellulosic biomass feedstocks with near-infrared spectroscopy, *Biotechnol. Biofuels* 8 (2015) 43.
- [20] L.M.L. Laurens, E.J. Wolfrum, High-throughput quantitative biochemical characterization of algal biomass by NIR spectroscopy; multiple linear regression and multivariate linear regression analysis, *J. Agric. Food Chem.* 61 (2013) 12307–12314.
- [21] D. Cozzolino, Use of infrared spectroscopy for in-field measurement and phenotyping of plant properties: instrumentation, data analysis, and examples, *Appl. Spectrosc. Rev.* 49 (2014) 564–584.
- [22] R. Lugassi, N. Goldshleger, A. Chudnovsky, Studying vegetation salinity: from the field view to a satellite-based perspective, *Remote Sens.* 9 (2017) 122.
- [23] A. Robic, D. Bertrand, J.F. Sassi, Y. Lerat, M. Lahaye, Determination of the chemical composition of Ulvan, a cell wall polysaccharide from *Ulva* spp. (ulvales, chlorophyta) by FT-IR and chemometrics, *J. Appl. Phycol.* 21 (2009) 451–456.
- [24] S. Shefer, A. Israel, A. Golberg, A. Chudnovsky, Carbohydrate-based phenotyping of the green macroalga *Ulva fasciata* using near infrared spectrometry: potential implications to marine biorefinery, *Bot. Mar.* 141 (2017) 1437–14323.
- [25] P.S. Waggoner, H.G. Craighead, Micro- and nanomechanical sensors for environmental, chemical, and biological detection, *Lab Chip* 7 (2007) 1238–1255.
- [26] W.M. Zhang, K.M. Hu, Z.K. Peng, G. Meng, Tunable micro- and nanomechanical resonators, *Sensors* 15 (2015) 26478–26566.
- [27] R. Jiang, Y. Linzon, E. Vitkin, Z. Yakhini, A. Chudnovsky, A. Golberg, Thermochemical hydrolysis of macroalgae *Ulva* for biorefinery: Taguchi robust design method, *Sci. Rep.* 6 (2016) 27761.
- [28] B. Ilic, H.G. Craighead, S. Krylov, W. Senaratne, C. Ober, P. Neuzil, Attogram detection using nanoelectromechanical oscillators, *J. Appl. Phys.* 95 (2004) 3694–3703.
- [29] S. Fanget, S. Hentz, P. Puget, J. Arcamone, M. Matheron, E. Colinet, P. Andreucci, L. Duraffourg, E. Meyers, M.L. Roukes, Gas sensors based on gravimetric detection – a review, *Sens. Actuators B: Chem.* 160 (2011) 804–821.
- [30] M.S. Hanay, S. Kelber, A.K. Naik, D. Chi, S. Hentz, E.C. Bullard, E. Colinet, L. Duraffourg, M.L. Roukes, Single-protein nanomechanical mass spectrometry in real time, *Nat. Nanotechnol.* 7 (2012) 602–608.
- [31] J. Toledo, V. Ruiz-Diez, G. Pfusterschmied, U. Schmid, J.L. Sanchez-Rojas, Flow-through sensor based on piezoelectric MEMS resonator for the in-line monitoring of wine fermentation, *Sens. Actuators B: Chem.* 254 (2018) 291–298.
- [32] M. Li, E.B. Myers, H.X. Tang, S.J. Aldridge, H.C. McCaig, J.J. Whiting, R.J. Simonson, N.S. Lewis, M.L. Roukes, Nanoelectromechanical resonator arrays for ultrafast, gas-phase chromatographic chemical analysis, *Nano Lett.* 10 (2010) 3899–3903.
- [33] J.L. Arlett, E.B. Myers, M.L. Roukes, Comparative advantages of mechanical biosensors, *Nat. Nanotechnol.* 6 (2011) 203–215.
- [34] K.L. Ekinci, Y.T. Yang, M.L. Roukes, Ultimate limits to inertial mass sensing based upon nanoelectromechanical systems, *J. Appl. Phys.* 95 (2004) 2682–2689.
- [35] J.L. Arlett, M.L. Roukes, Ultimate and practical limits of fluid-based mass detection with suspended microchannel resonators, *J. Appl. Phys.* 108 (2010) 084701.
- [36] Y. Linzon, B. Ilic, S. Lulinsky, S. Krylov, Efficient parametric excitation of silicon-on-insulator microcantilever beams by fringing electrostatic fields, *J. Appl. Phys.* 113 (2013) 163508.
- [37] Y. Linzon, S. Krylov, B. Ilic, D.R. Southworth, R.A. Barton, B.R. Cipriani, J.D. Cross, J.M. Parpia, H.G. Craighead, Real-time synchronous imaging of electromechanical resonator mode and equilibrium profiles, *Opt. Lett.* 35 (2010) 2654–2656.
- [38] S. Mahajne, D. Guetta, S. Lulinsky, S. Krylov, Y. Linzon, Liquid mass sensing using resonating microplates under harsh drop and spray conditions, *Phys. Res. Int.* 2014 (2014) 320324.
- [39] F. Fernand, A. Israel, J. Skjermo, T. Wichard, K.R. Timmermans, A. Golberg, Offshore macroalgae biomass for bioenergy production: environmental aspects, technological achievements and challenges, *Renew. Sustain. Energy Rev.* 75 (2017) 35–45.
- [40] W.C. ASTM International, Standard Test Method for Determination of Carbohydrates in Biomass by High Performance Liquid Chromatography, ASTM International, West Conshohocken, PA, 2015 [www.astm.org](http://www.astm.org).
- [41] S.J. Adams, Dust deposition and measurement: a modified approach, *Environ. Technol.* 18 (1997) 345–350.
- [42] S.J. Adams, D. Ford, Monitoring of deposited particles in cultural properties: the influence of visitors, *Atmos. Environ.* 35 (2001) 4073–4080.
- [43] A. Chudnovsky, E. Ben-Dor, E. Paz, Using near infrared spectroscopy for rapid quantification of sediment dust in the indoor environment, *J. Near Infrared Spectrosc.* 15 (2007) 59–70.
- [44] P. Williams, Near-infrared Technology – Getting the Best Out of Light, 2nd ed., Value Added Wheat, Canada, 2003.
- [45] K. Esbensen (Ed.), Multivariate Data Analyses, An Introduction to Multivariate Data Analyses and Experimental Design, Alborg University, CAMO, 2002.
- [46] P.J. Curran, J.L. Dungan, B.A. Macler, S.E. Plummer, D.L. Peterson, Reflectance spectroscopy of fresh whole leaves for estimation of chemical concentration, *Remote Sens. Environ.* 39 (2015) 153–166.
- [47] G.R. Hunt, Spectral signatures of particulate minerals, in the visible and near-infrared, *Geophysics* 42 (1977) 501–513.
- [48] G.R. Hunt (Ed.), Spectroscopic Properties of Rocks and Minerals in Handbook of Physical properties of Rocks, vol. I, CRC Press, Boca Raton, 1982.
- [49] S.J. Gaffey, L.A. McFadden, D. Nash, C.M. Pieters (Eds.), Ultraviolet, Visible, and Near-infrared Reflectance Spectroscopy: Laboratory spectra of Geologic Materials: Remote Geochemical Analysis: Elemental and Mineralogical Composition, Cambridge University Press, Cambridge, 1993.
- [50] C.S. Daughtry, Discriminating crop residues from soil by shortwave infrared reflectance, *Agron. J.* 93 (2001) 125–131.
- [51] J. Toledo, T. Manzaneque, V. Ruiz-Diez, M. Kucera, G. Pfusterschmied, E. Wistrela, U. Schmid, J. Sánchez-Rojas, Piezoelectric resonators and an oscillator circuit based on higher-order out-of-plane modes for density-viscosity measurements of liquids, *J. Micromech. Microeng.* 26 (2016).
- [52] J. Toledo, V. Ruiz-Diez, G. Pfusterschmied, U. Schmid, J. Sánchez-Rojas, Characterization of oscillator circuits for monitoring the density-viscosity of liquids by means of piezoelectric MEMS microresonators, *Proceedings of SPIE – The International Society for Optical Engineering: Smart Sensors, Actuators, and MEMS VIII Conference (Barcelona, Spain)* (2017).
- [53] J.B. Adams, M.O. Smith, P.I. Johnson, Spectral mixture modeling: a new analysis of rock and soil types at the Viking Lander 1 site, *J. Geophys. Res.* 91 (1986) 8098–8112.
- [54] N. Keshava, J.F. Mustard, Spectral unmixing, *IEEE Signal Process. Mag.* 19 (2002) 44–57.
- [55] A. Chudnovsky, E. Ben-Dor, A.B. Kostinski, I. Koren, Mineral content analysis of atmospheric dust using hyperspectral information from space, *Geophys. Res. Lett.* 36 (2009) L15811.